44th AIAA Aerospace Sciences Meeting and Exhibit, January 9–12, 2006 Reno, Nevada

Application of the Time Spectral Method to Periodic Unsteady Vortex Shedding

Arathi K. Gopinath*, and Antony Jameson†
Stanford University, Stanford, CA 94305-4035

The Time Spectral method has been proposed for the fast and efficient computation of periodic unsteady flows. The algorithm has been validated with both 2D and 3D test cases and applied successfully for internal and external aerodynamics. It has shown tremendous potential for reducing the computational cost compared to conventional time-accurate methods, by enforcing periodicity and using Fourier representation in time, leading to spectral accuracy. Until now, the algorithm could be used only for flows where the frequency of unsteadiness was known a priori. In this paper, we propose a method to compute the time period as part of the solution to the unsteady problem, in cases where the frequency of unsteadiness is not predefined.

I. INTRODUCTION

Although most aerodynamic flows are treated as steady ones, many others are non-stationary. The variety of non-stationary flows is large, and includes transient regimes, impulsive starts, maneuvering, periodic flows and flows that are intrinsically unsteady because of the mechanism of vortex shedding from bluff bodies. One category of unsteady problems of oscillatory type are forced oscillations where the unsteadiness in the flow is caused by the periodic motion of the body. Practical examples of this type include helicopter rotor blades in forward flight, rotor-stator combinations in turbomachinery, wind turbine rotors and flapping wing propulsion systems.

Wakes behind bluff bodies are unsteady(and sometimes periodic) under most conditions. Simple geometries like the circular cylinder and the sphere have been investigated for a long time, in order to understand the physics of flow separation and vortex formation. A better understanding of these flows is important as it relates to several practical applications in the form of base drag reduction on cars, trucks, aircraft afterbodies and other vehicles. Delta wings, pointed cylinders and prolate spheroids are some examples where the behavior of the body is related to the dynamics of the vortices released from the body surface. The periodic unsteadiness in these flows(e.g. vortex shedding at regular intervals) does not occur at predefined frequencies as in the case of a pitching airfoil/wing.

Though the topic of unsteady flows has been studied for decades via experiments, predicting these flows using Computational Fluid Dynamics in a cost-effective way, is still a severe challenge. When time accurate solvers like the implicit second-order Backward Difference Formula(BDF) are used to treat periodic flows, the governing equations are integrated in time until the periodic steady state is reached. This may require integrations over 5 or more cycles for a typical pitching motion. We proposed the Time Spectral algorithm[1]

*Doctoral Candidate, AIAA Student Member.
†Thomas V. Jones Professor of Engineering, Department of Aeronautics and Astronautics, AIAA Member

to solve time-periodic unsteady problems, following the direction suggested by Hall et.al.[2] Compared to the dual time stepping BDF, applicable for arbitrary time histories, this algorithm showed significant reduction in CPU requirements for time periodic flows. A Fourier representation was used for time discretization, leading to spectral accuracy. Moreover periodicity was directly enforced and hence the solution did not have to evolve through transients to reach a periodic steady-state. The method has been applied successfully to both two- and three-dimensional unsteady flows like analysis of Vertical-Axis Wind-Turbines[3] to study the dynamic motion of a turbine blade spinning about an axis and for turbomachinery problems.[4] All these applications fall into the first category of periodic unsteady flows where the unsteady frequency is known a priori.

In this paper, we will computationally predict the unsteady flows that fall into the second category, where the flow is indeed periodic, but the frequency is not predetermined. McMullen et.al.[5] proposed the Gradient Based Variable Time Period(GBVTP) method, in combination with the Nonlinear frequency domain method, which iteratively solves for the time period during the process of solving the governing equations. We will use a similar approach, in combination with the Time Spectral method.

In the following sections, we will first repeat the formulation of the Time Spectral Method[1] for clarity. We will discuss the stability of the algorithm as in[4] and then formulate the gradient based approach to computing the time period of the periodic unsteady problem. In the results section, we will present our results of laminar vortex shedding behind cylinders with validation and then present detailed results of laminar flow over NACA0012 airfoil at 20 degrees angle of attack exhibiting a complex interaction between vortices shed forming a shear layer. The studies focus on low Reynolds number flows in order to isolate the basic numerical aspects of the algorithm development from the turbulence modelling issues, since the simulation of separated flows could be very sensitive to the turbulence model. We will end the paper with conclusions and future work.

II. MATHEMATICAL FORMULATION

A. The Time Spectral Method

The Time Spectral Method was originally proposed and validated in.[1] The algorithm takes advantage of the periodic nature of the problem, and uses a Fourier representation in time making it possible to achieve spectral accuracy.

The governing equations in integral form are given by

$$\int_{\Omega} \frac{\partial w}{\partial t}\, dV + \oint_{\partial\Omega} \vec{F} \cdot \vec{N}\, ds = 0. \tag{1}$$

In semi-discrete form, the unsteady equations in Cartesian coordinates can be written as

$$V\frac{\partial w}{\partial t} + R(w) = 0, \qquad R(w) = \frac{\partial}{\partial x_i} f_i(w), \tag{2}$$

The discrete fourier transform of w, for a time period T, is given by

$$\hat{w}_k = \frac{1}{N}\sum_{n=0}^{N-1} w^n e^{-ik\frac{2\pi}{T}n\Delta t}$$

and its inverse transform,

$$w^n = \sum_{k=-\frac{N}{2}}^{\frac{N}{2}-1} \hat{w}_k e^{ikn\frac{2\pi}{T}\Delta t}, \tag{3}$$

where the time period T is divided into N time intervals(N even), $\Delta t = T/N$.

Discretize the governing equations as a pseudo-spectral scheme,

$$V D_t w^n + R(w^n) = 0. \tag{4}$$

McMullen et.al.[6,5]solved the time accurate equations in Eq.(4) by transforming them into frequency domain and introducing a pseudo-time t^*, like in the case of the dual time stepping scheme,

$$V \frac{\partial \hat{w}_k}{\partial t_k^*} + V \frac{2\pi}{T} ik\hat{w}_k + \hat{R}_k = 0. \tag{5}$$

Alternatively, the Time Spectral Algorithm solves the governing equations in the time-domain, considerably gaining on the computational cost required to transform back and forth to the frequency domain. From Eq.(3), the time discretization operator D_t can be written as

$$D_t w^n = \frac{2\pi}{T} \sum_{k=-\frac{N}{2}}^{\frac{N}{2}-1} ik\hat{w}_k e^{ik\frac{2\pi}{T}n\Delta t}. \tag{6}$$

This summation involving the fourier modes $\hat{w}_k$, can be rewritten in terms of the conservative variables w in the time domain, both for even and odd N as(see Appedix for derivation for a function with period 2π),

$$D_t^{even} w^n = \frac{2\pi}{T} \sum_{m=-\frac{N}{2}+1}^{\frac{N}{2}-1} d_m^{even} w^{n+m},$$

and

$$D_t^{odd} w^n = \frac{2\pi}{T} \sum_{m=\frac{1-N}{2}}^{\frac{N-1}{2}} d_m^{odd} w^{n+m}, \tag{7}$$

where

$$d_m^{even} = \begin{cases} \frac{1}{2}(-1)^{m+1} \cot(\frac{\pi m}{N}) & : \quad m \neq 0 \\ 0 & : \quad m = 0 \end{cases}$$

and

$$d_m^{odd} = \begin{cases} \frac{1}{2}(-1)^{m+1} cosec(\frac{\pi m}{N}) & : \quad m \neq 0 \\ 0 & : \quad m = 0 \end{cases} \tag{8}$$

Note that $d_{-m} = -d_m$ for both even and odd N. Hence D_t takes the form of a central difference operator connecting all the time levels, yielding an integrated space-time formulation which requires the simultaneous solution of the equations for all time levels. A pseudo-time t^* is introduced as in the dual-time stepping case, and the equations are time marched to a periodic steady-state

$$V \frac{\partial w^n}{\partial t^*} + V D_t w^n + R(w^n) = 0. \tag{9}$$

The algorithm has been implemented in cell-centered semi-discrete finite volume schemes on structrured grids. A full W-cycle multigrid algorithm has been used to accelerate convergence, where a pseudo time step with a five-stage Runge-Kutta scheme is performed at each level. The method is amenable to parallel processing and has been used for both Euler and RANS calculations.

B. Stability

The addition of the time derivative term $D_t w$ in equation (9) must be taken into account in the definition of the pseudo-time step Δt^*, in comparison with solving a steady-state problem.

Recall Eq. 5

$$V\frac{\partial \hat{w}_k}{\partial t_k^*} + V\frac{2\pi}{T}ik\hat{w}_k + \hat{R}_k = 0,$$

where t_k^* is the pseudo-time for wave number k. Note that the orthogonality of the Fourier coefficients ensures that the equations corresponding to each wave number are decoupled. From a stability analysis for the frequency domain method, the pseudo-time step Δt_k^* can be estimated to be

$$\Delta t_k^* = \frac{CFL * V}{||\lambda|| + k' * V}, \tag{10}$$

where V is the volume of a cell, $||\lambda||$ is the spectral radius of the flux Jacobian of the spatial part of the equations and $k' = k * \frac{2\pi}{T}$. I.e. an additional term based on the wave number is added to the denominator of equation (10) compared to the standard time step definition for a steady-state problem. Hence the pseudo-time step is based on the wave number for each frequency and thus different for every frequency.

To estimate a frequency-based pseudo-time step limit for the Time Spectral Method that is solved in the time domain, consider the inverse fourier transform of equation (5) back to the time domain,

$$F^{-1}(V\frac{\Delta \hat{w}_k}{\Delta t_k^*} + V\frac{2\pi}{T}ik\hat{w}_k + \hat{R}_k) = 0. \tag{11}$$

or

$$F^{-1}(V\frac{\Delta \hat{w}_k}{\Delta t_k^*}) + V\frac{\partial w}{\partial t} + R(w) = 0. \tag{12}$$

This inverse fourier transform operation with different time steps Δt_k^* in the frequency domain, will transform to a matrix time step in the time domain coupling all the time levels. As the spectral radius varies from cell to cell, this matrix will have to be inverted in each cell and at every stage of the multigrid cycle, which makes this approach rather costly.

Alternatively, it is possible to use a constant time-step in the frequency domain corresponding to the largest wave number, i.e. the most restrictive time-step. Then,

$$\Delta t_k^* = \frac{CFL * V}{||\lambda|| + k' * V} \tag{13}$$

where

$$k' = \begin{cases} \frac{N}{2} * \frac{2\pi}{T} & : \quad N \text{ is even} \\ \frac{N-1}{2} * \frac{2\pi}{T} & : \quad N \text{ is odd} \end{cases} \tag{14}$$

On transforming back to the time domain, the time-step for each time instance is constant and retains the form of Δt_k^* since it is independent of the wave-numbers. The choice of time-step (14) is rather restrictive, especially when the number of time intervals increases. However it considerably reduces the computational cost involved in inverting a matrix several times.

C. Odd-Even decoupling

Eq. (7) can be written as a matrix vector multiplication

$$D_t w = DW, \tag{15}$$

where $W = (w^1, w^2, \cdots, w^N)^T$ and the matrix D is given by

$$D^{even} = \begin{pmatrix} 0 & d_1^{even} & \cdots & d_{\frac{N}{2}-1}^{even} & 0 & -d_{\frac{N}{2}-1}^{even} & \cdots & -d_1^{even} \\ -d_1^{even} & 0 & d_1^{even} & d_2^{even} & \cdots & 0 & \cdots & -d_2^{even} \\ \vdots & \vdots & \vdots & \vdots & \vdots & \vdots & \vdots & \vdots \\ d_1^{even} & d_2^{even} & \cdots & 0 & \cdots & -d_2^{even} & -d_1^{even} & 0 \end{pmatrix} \tag{16}$$

for an even number of time intervals and by

$$D^{odd} = \begin{pmatrix} 0 & d_1^{odd} & \cdots & d_{\frac{N-1}{2}}^{odd} & -d_{\frac{N-1}{2}}^{odd} & \cdots & -d_1^{odd} \\ -d_1^{odd} & 0 & d_1^{odd} & d_2^{odd} & \cdots & \cdots & -d_2^{odd} \\ \vdots & \vdots & \vdots & \vdots & \vdots & \vdots & \vdots \\ d_1^{odd} & d_2^{odd} & \cdots & \cdots & -d_2^{odd} & -d_1^{odd} & 0 \end{pmatrix} \tag{17}$$

for an odd number of time intervals. From equation (16) it is clear that every row of D^{even} contains two zeros, while the rows of D^{odd} only have one. As a consequence D^{even} has two zero eigenvalues with eigenvectors $e_1 = (1, 1, \cdots, 1)^T$ and $e_2 = (1, 0, 1, 0, \cdots, 1, 0)^T$. Eigenvector e_1 corresponds to a zero time derivative for a constant solution, a property of a consistent scheme. However also eigenvector e_2 results in a discrete zero time-derivative, while e_2 clearly corresponds to an odd-even decoupled solution, i.e. this mode is not damped by D^{even}.

D^{odd} on the other hand only has one zero eigenvalue with corresponding eigenvector $e_1 = (1, 1, \cdots, 1)^T$. Consequently the odd-even decoupled solution does not lead to a discrete zero time-derivative for D^{odd}.

It was found that for cases where the time derivative is relatively small both D^{even} and D^{odd} are stable, e.g. pitching airfoils and wings at small forced frequencies.[1] However for problems where the time derivative is important, e.g. high RPM turbomachinery problems,[4] the odd-even decoupling introduces instabilities, which may lead to failure of the algorithm using an even number of time intervals.

D. Gradient Based Method for Computing the Time Period

For the class of periodic problems for which the time period is not predetermined, we propose a gradient based method for computing the exact time period iteratively starting from an initial guess. This method is analogous to the Gradient Based Variable Time Period(GBVTP) method proposed by McMullen et.al.[5] for the Frequency Domain method.

The main concept in this method is based on the fact that the unsteady governing equations Eq.(4) rewritten as $G(w) = 0$, will have a solution, or in the words, will converge numerically, only when the equations are discretized with the exact time period(TP*) of the unsteadiness. Hence, for different guesses of the time period, the residuals will converge to different levels of accuracy. As the guess gets closer and closer to TP*, the residuals will converge further and only at TP* will the residuals go to machine zero and solve for $G(w) = 0$ exactly.

In effect, the residuals and their gradients with respect to the time period have the information we need. Our aim is to compute TP* as part of the solution and hence the time period will no longer be held fixed as in the case of problems where the time period is known apriori. It will be included as a variable to be computed as part of the solution. Thus we will have to solve for $G(w, T) = 0$. We will pose this as an optimization problem where the zero of the unsteady residuals Eq.(4) will be sought.

Let us introduce a figure of merit,

$$I^n = V \frac{2\pi}{T} \sum_m d_m w^{n+m} + R(w^n) \tag{18}$$

and take the gradient of the square of I^n with respect to T,

$$\frac{1}{2}\frac{\partial {I^n}^2}{\partial T} = I^n * V \frac{-2\pi}{T^2} \sum_m d_m w^{n+m}. \tag{19}$$

The average of all the gradients over the entire time period and over all the control volumes will be used to update the time period for the next iteration.

$$T^{k+1} = T^k - \Delta T \frac{\partial I^2}{\partial T} \tag{20}$$

A suitable stable ΔT will be chosen to guarantee convergence. Starting with an initial guess, the governing equations are marched to a periodic steady state. Typically if the initial guess is not exactly equal to TP*, the residuals will stall at some finite level after the initial transients die down. At this point, the gradient is computed as in Eq.(19) and the time period modified for the next iteration. This is repeated at every iteration, while simultaneously updating w for the modified time period, until the residuals and an estimate of the time period have reached the desired level of accuracy.

III. Current Results

In the following subsections we will present results from numerical simulations of the RANS equations for two different two-dimensional test cases of laminar flow. The experimental data is for incompressible flow. Since our solver is for compressible flows, the calculations were carried out for a Mach number of 0.2. One of the test cases is laminar vortex shedding behind circular cylinders at Re=180. The other is the periodic vortex shedding behind a NACA0012 airfoil at high angles of attack at Re=1000. Comparison with experimental and computational results will be provided as appropriate.

In cases where the unsteady effects are large, Van der Weide et.al.[4] have shown that using even number of time intervals in combination with Time Spectral method could cause odd-even decoupling which would eventually destabilise the system. The odd number of time intervals formulation has alleviated this problem in these cases. Hence, for both our test cases, we will use odd number of time intervals.

A. Cylinder Flow

At Reynolds numbers between 49 and 194,[7] vortices are shed alternately behind circular cylinders in a two-dimensional fashion called the Karman vortex street. This case presents itself as a good example of periodic unsteadiness in the flow which has not been forced, but has been caused by instabilities in the shear layer of the flow. Hence, the time period of the periodic phenomenon is not known apriori. The large database of experimental and computational results makes it an invaluable test case for validation purposes.

The grid used for this test case is an externally generated "O-mesh" with 256x128 points in the circumferential and radial directions respectively. The mesh boundary is 200 diameters away from the center of the cylinder. The first cell spacing is about 1E-3 diameters and an exponential stretching function stretches the grid in the radial direction upto the boundary. The near resolution features of the mesh is shown in Fig. 1(a). We choose a relatively high Reynolds number(Re=180) within the range of Reynolds numbers at which a two- dimensional Karman vortex street is observed. It has been shown by previous investigators[5] that as the Reynolds number is increased, more and more harmonics will be needed to capture the unsteady phenomenon.

Table 1 lists the coefficient of drag(C_d), coefficient of base suction pressure(C_{pb}) and the Strouhal number predicted by various investigators in the past. Williamson's[8,9] experimental results are fit through a "universal curve" that relates Strouhal number to Reynolds number and C_{pb} to Reynolds number in the

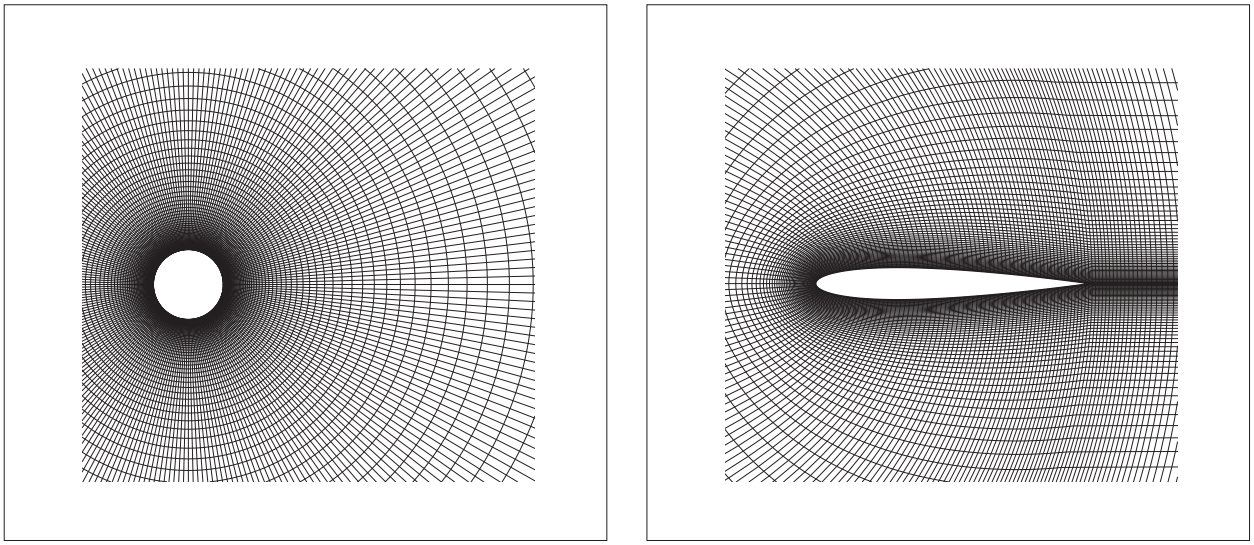

(a) Cylinder Flow - O mesh

(b) High Alpha Airfoil - C mesh

Figure 1.

Experiment	$-C_{pb}$	C_d	St
Williamson[8,9]	0.9198		0.1919
Roshko[10]			0.185
Henderson[11]	0.9599	1.336	

Table 1. Time-Averaged coefficients and Strouhal number from previous investigators

#Time Intervals	$-C_{pb}$	C_d	St
5	.9203	1.3324	.1884
7	.9258	1.3339	.1865
9	.9332	1.3392	.1866
11	.9348	1.3404	.1867
13	.9351	1.3406	.1866
21	.9351	1.3406	.1866

Table 2. Time-Averaged coefficients and Strouhal number computed with various #Time Intervals

range $49 < Re < 180$ where parallel vortex shedding is observed. The fits are reported to be accurate within $+/-2\%$. Table 2 lists similar data predicted by the Time Spectral method using varying amounts of temporal resolution. Temporal convergence is exhibited and it is also observed that 9 time intervals, or 4 harmonics are sufficient to predict the global coefficients to engineering accuracy. This fact is further strengthened by the plots in Fig. 2 (a) and (b) which demonstrate the variation of C_d and C_{pb} over one time period with varying temporal resolution. Our time averaged coefficient results also seem to closely match results from Henderson[11] who has used spectral element methods based on 8th order accurate polynomials.

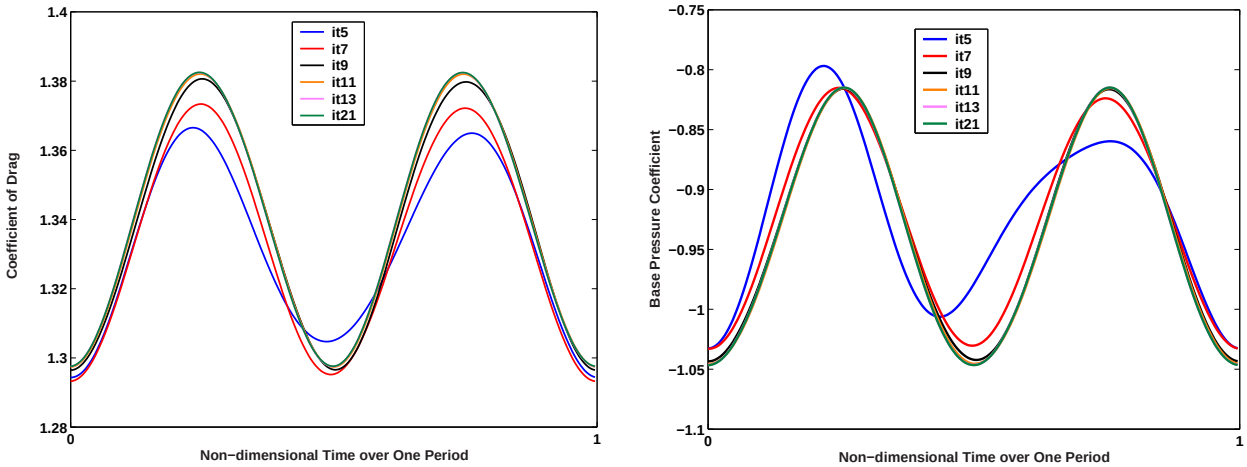

(a) Coefficient of Drag

(b) Coefficient of Base suction Pressure

Figure 2. Cylinder flow : Variation of C_d and C_{pb} over one period using varying temporal resolution

In order to start the unsteady process without having to wait for round-off errors to introduce disturbances, the cylinder is rotated in a sinusoidal manner at the frequency of the initial guess with an amplitude of 1 degree for about 10 MG cycles. The computation is started with an initial guess close to the experimental Strouhal number and run until the initial transients died down. Then the gradient based modification of the time period is introduced and repeated until desired level of accuracy is attained.

Fig. 3 shows entropy contours in the wake of the cylinder at various time instances over one period. Similarly, Fig. 4 shows streamtraces colored with the local Mach numbers. These figures clearly show the vortices that are shed alternately behind the cylinder forming the Karman vortex street.

B. High Angle of Attack Airfoil

The viscous flow over a NACA0012 airfoil at Re=1000 fixed at 20 degrees angle of attack shows periodic vortex shedding with a huge shear layer zone on the suction side of the airfoil surface. This case poses as an interesting test case for the Time Spectral approach in combination with computing the time period. The detail of the "C-mesh" used for this computation is shown in Fig. 1(b). It is a 256x64 mesh generated using conformal mapping. The first cell spacing of the grid is 1E-4 chords.

Similar to the cylinder case, starting with an initial guess(based on results from previous investigators[12]), we will proceed with the computation using a fixed time period until some residual level. The transition to limiting shedding cycle will be accelerated with a couple of initial pitches of the airfoil with an amplitude of .5 degrees about a mean of 20 degrees. Then, the gradient based alteration of the time period is introduced

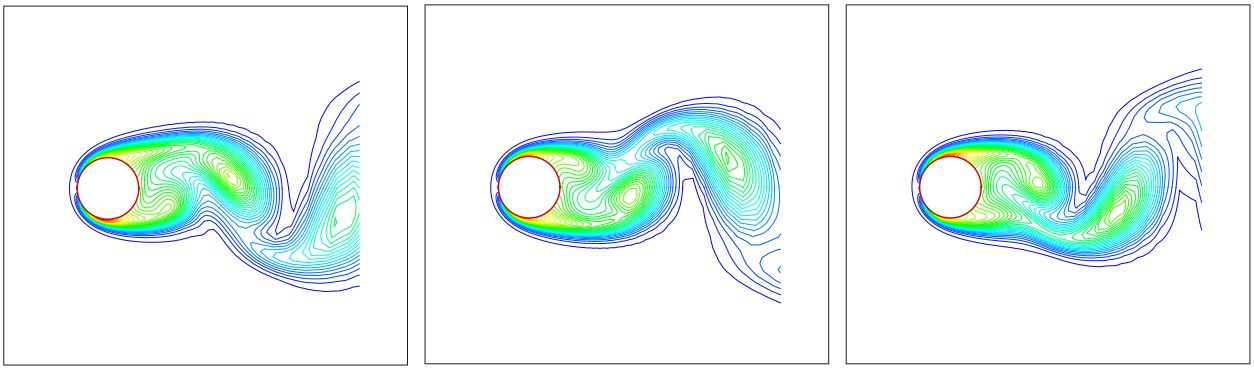

(a) t = 0 (b) t = $\frac{T}{3}$ (c) t = $\frac{2T}{3}$

Figure 3. Cylinder flow : Entropy contours at various time instances over one period

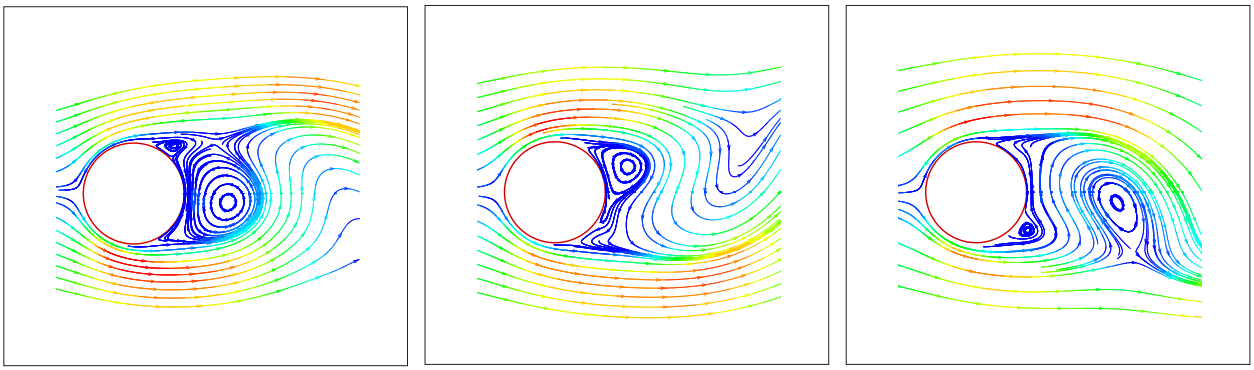

(a) t = 0 (b) t = $\frac{T}{3}$ (c) t = $\frac{2T}{3}$

Figure 4. Cylinder flow : Streamtraces colored by Mach number at various time instances over one period

to achieve a desired level of accuracy both for the unsteady solution and the estimate of the exact time period(TP*).

Fig. 5 shows convergence to the exact time period starting from the initial guess using various levels of temporal resolution. Note that as the number of time intervals is increased, the converged time period gets closer to TP*,i.e. temporal convergence is achieved. Atleast 9 time intervals are required to predict TP* to engineering accuracy. Fig. 6 shows the error in the computed time period using varying number of time intervals per period, based on TP* computed with $N = 21$. It proves that close to exponential convergence has been achieved which is evidenced from the linear variation of the error on a semi-log plot.

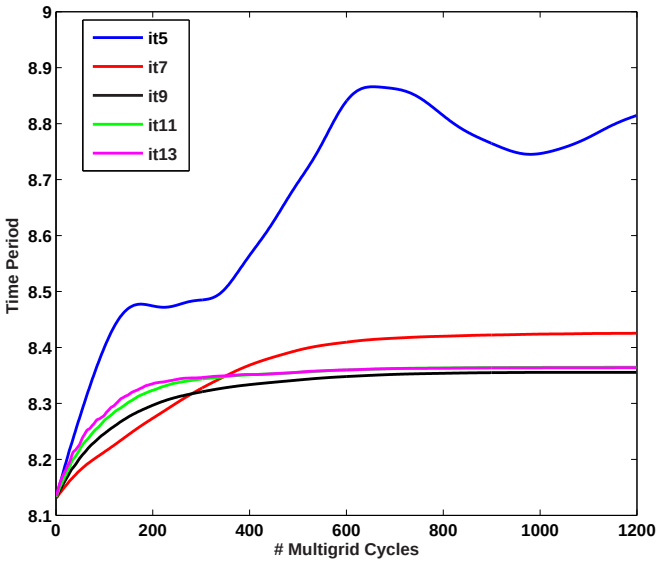

Figure 5. High Alpha NACA0012 case : Convergence from initial guess to exact Time Period with varying temporal resolution

The observation that $N = 9$ is all that is required to achieve engineering accuracy is further affirmed by the plots showing variation of Coefficient of Drag(Fig. 7(a)) and Coefficient of Lift(Fig. 7(b)) over one period computed using varying N.

Another set of results were assimilated based on different starting guesses for the time period. All of them were simulated with $N = 9$ and Fig. 8 shows their convergence to the same time period using the gradient based approach. The percentages listed are the differences in percentage between the exact time period and the initial guess. This trend eliminates any random results that can occur with a single initial guess computation.

Fig. 9 shows convergence trends of the solution of unsteady residuals while holding the time period fixed and using 11 time intervals. With an approximate time period 2.75% different from TP*, the solution converges 3 orders of magnitude and stalls. With a time period computed using the gradient based approach and accurate upto 6 orders of magnitude, the residuals converge further and saturate at 6 orders of magnitude. Also shown is a computation with time period 7.5% different from TP* which saturates at a higher level of accuracy. This confirms that the accuracy of the time period of periodic unsteadiness directly dictates the level of accuracy of the unsteady residuals of the discrete system of equations.

Fig. 10 shows entropy contours at various time instances over one period. Similarly, Fig. 11 shows streamtraces colored with the local Mach numbers. These figures clearly show the vortices shed periodically

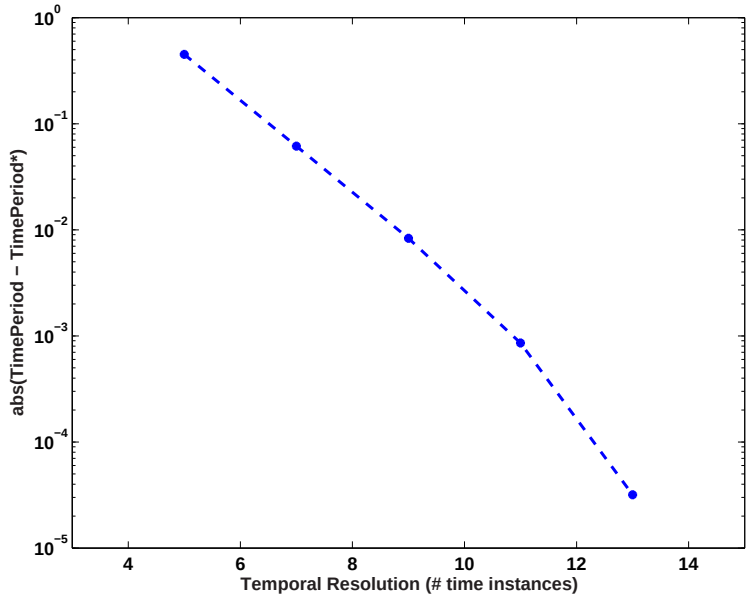

Figure 6. High Alpha NACA0012 case : Variation of error between computed and exact time period using varying temporal resolution

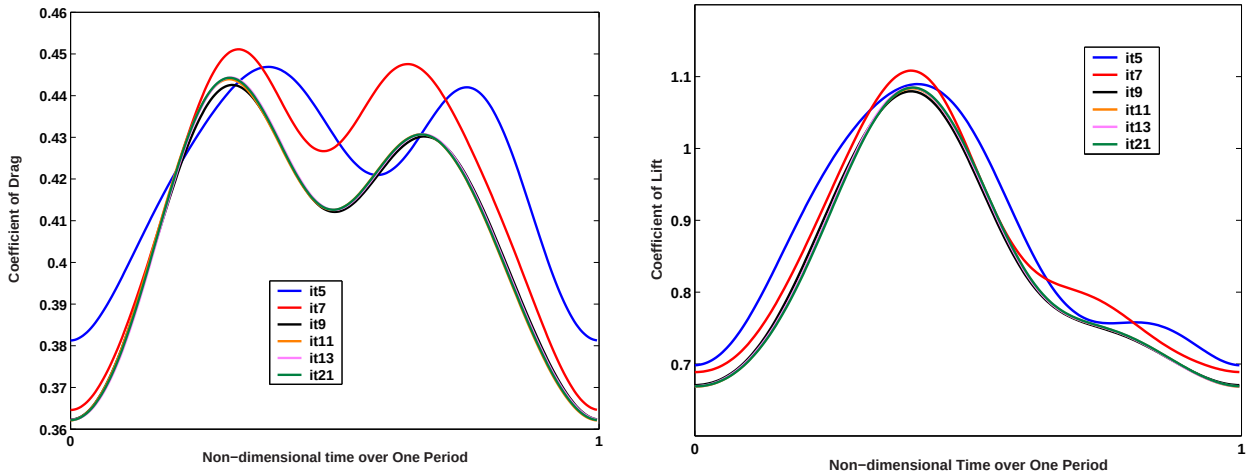

(a) Coefficient of Drag

(b) Coefficient of Lift

Figure 7. High Alpha NACA0012 : Variation of C_d and C_l over one period using varying temporal resolution

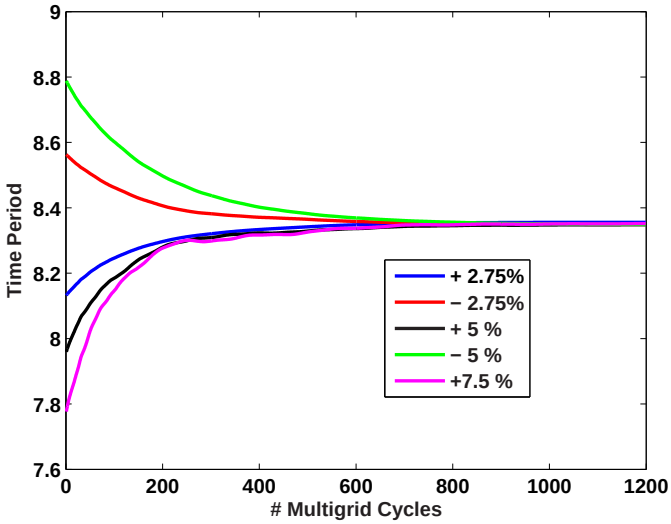

Figure 8. High Alpha NACA0012 Case : Various time period starting guesses converging to same exact time period

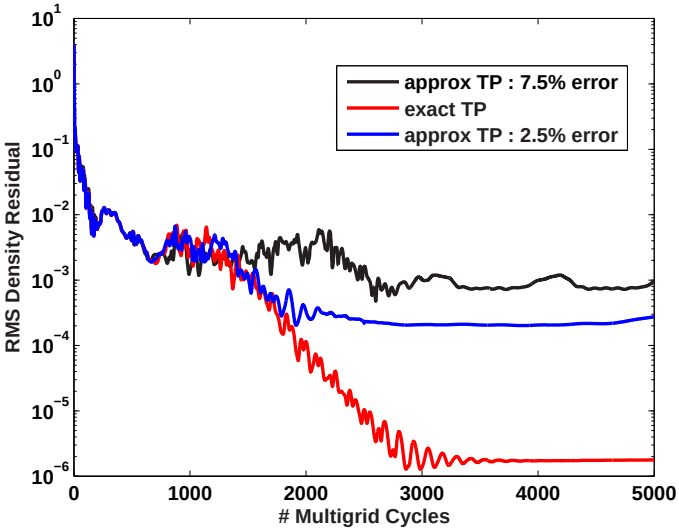

Figure 9. High Alpha NACA0012 Case : Convergence of RMS Density Residual with approx and exact time period

on the suction side of the airfoil creating a huge shear layer. Vortices are shed from the leading edge and trailing edge and a complex interaction is observed in the shear layer characterized by several frequencies in one time period. This is also depicted in the C_l and C_d plots where their variation is more complex than a sinusoid that was observed in the cylinder case.

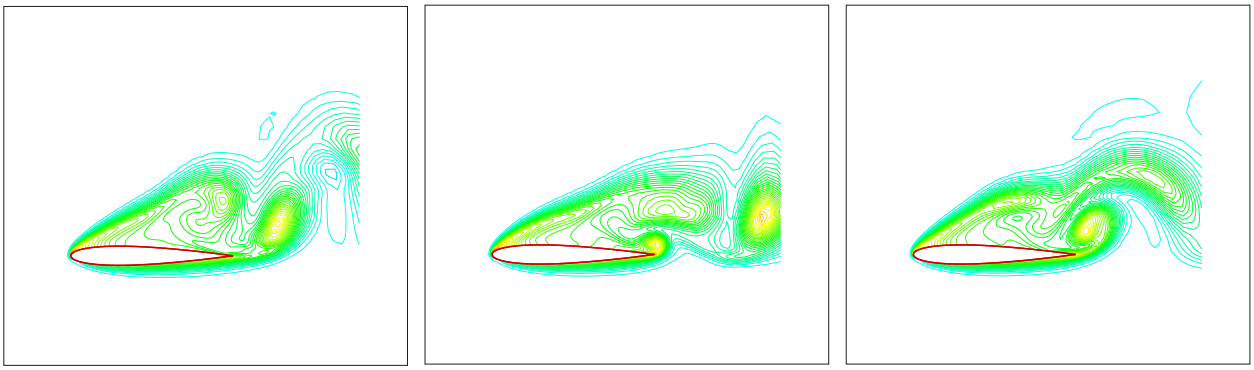

(a) t = 0 (b) t = $\frac{T}{3}$ (c) t = $\frac{2T}{3}$

Figure 10. High Alpha NACA0012 : Entropy contours at various time instances over one period

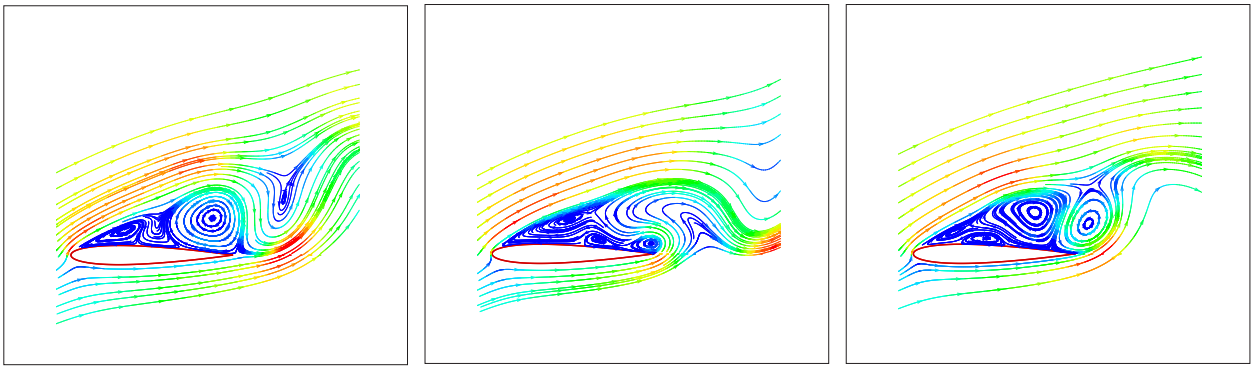

(a) t = 0 (b) t = $\frac{T}{3}$ (c) t = $\frac{2T}{3}$

Figure 11. High Alpha NACA0012 : Streamtraces colored by Mach number at various time instances over one period

IV. Conclusions and Future Work

The Time Spectral method has been previously shown to be efficient and accurate for periodic unsteady flows that are forced and the frequency of unsteadiness is predetermined. In this paper, we have made an attempt to extend and modify this algorithm to the other class of periodic unsteady problems where the time period is unknown a priori. A gradient based approach has been chosen which drives the unsteady residuals to machine zero while simultaneously updating the time period. Results with validation have been reported for vortex shedding behind circular cylinders and detailed computational results presented for a NACA0012 airfoil at 20 degrees angle of attack at Re=1000. The periodic unsteady shedding of vortices in both the test cases have been accurately captured with small amount of temporal resolution. It has also been proved that

to get an accurate solution of the discretized equations, it is important to predict the time period to a similar level of accuracy. A small percentage of error could lead to a completely different solution. It is also necessary to use at least the minimum amount of temporal resolution needed to capture the unsteady phenomenon in order to predict the right time period. These two features will assure a machine-level accurate solution of the governing equations.

In the future, we would like to make this approach more robust by trying various other optimization strategies, better ways of providing an initial guess or providing not-so-close initial guesses and still obtain convergence, faster convergence, adaptively increasing the temporal resolution as needed etc. Artificial compressibility could be introduced in combination with a compressible solver to improve efficiency and accuracy. Adaptive mesh refinement could be introduced in order to capture the vortices better.

This is a first step towards predicting unsteady flows about high-lift single/multi-element airfoils/wings. Transonic test cases and realistic test conditions would be an ideal extension. Further, we would like to simulate the effect of unsteady blowing/suction by synthetic jets to reduce separation effects. The Time Spectral method with the capability of simulating both forced periodic unsteadiness and that caused by instabilities, would be a fit candidate for problems with complex interactions between forced and instability induced unsteadiness.

V. ACKNOWLEDGMENT

This work has benefited from the generous support of the Department of Energy under contract number LLNL B341491 as part of the Advanced Scientific Computing(ASC) program at Stanford University.

References

[1]A. Gopinath and A. Jameson. Time spectral method for periodic unsteady computations over two- and three-dimensional bodies. *AIAA paper 05-1220*, AIAA 43rd Aerospace Sciences Meeting and Exhibit, Reno, NV, January 10-13 2005.

[2]K.C. Hall, J.P. Thomas, and W.S. Clark. Computation of unsteady nonlinear flows in cascades using a harmonic balance technique. *AIAA Journal*, 40(5):879–886, May 2002.

[3]J.C.Vassberg, A.Gopinath, and A.Jameson. Revisiting the vertical-axis wind-turbine design using advanced computational fluid dynamics. *AIAA paper 05-0047*, 43rd AIAA Aerospace Sciences Meeting and Exhibit, Reno, NV, January 10-13 2005.

[4]E. Van der Weide, A. Gopinath, and A. Jameson. Turbomachinery applications with the time spectral method. *AIAA paper 05-4905*, 17th AIAA Computational Fluid Dynamics Conference, Toronto, Ontario, June 6-9 2005.

[5]M. McMullen, A. Jameson, and J.J. Alonso. Application of a non-linear frequency domain solver to the euler and navier-stokes equations. *AIAA paper 02-0120*, AIAA 40th Aerospace Sciences Meeting and Exhibit, Reno, NV, January 2002.

[6]M. McMullen, A. Jameson, and J.J. Alonso. Acceleration of convergence to a periodic steady state in turbomachinery flows. *AIAA paper 01-0152*, AIAA 39th Aerospace Sciences Meeting, Reno, NV, January 2001.

[7]C.H.K.Williamson. Vortex dynamics in the cylinder wake. Technical Report *28:477-539*, Annual Review Fluid Mech., 1996.

[8]C.H.K.Williamson. Defining a universal and contiguous strouhal-reynolds number relationship of the laminar vortex shedding of a circular cylinder. Technical Report *31:2747-2747*, Physics of Fluids, October 1988.

[9]C.H.K.Williamson. Measurements of base pressure in the wake of a cylinder at low reynolds numbers. Technical Report *14:pp.38-46*, Z.Flugwiss, Weltraumforsch,, 1990.

[10]A.Roshko. On the development of turbulent wakes from vortex streets. Technical report, NACA Technical Report 1191, NACA, January 1954.

[11]R.D.Henderson. Details of the drag curve near the onset of vortex shedding. Technical report, Physics of Fluids, 1995.

[12]A.A.Belov. A new implicit multigrid-driven algorithm for unsteady incompressible flow calculations on parallel computers. Technical report, Dissertation, Princeton University, June 1997.

[13]P.Moin. Me308 spectral methods in computational physics. Technical report, Class notes provided as part of Stanford's ME308 Course, 1997.

[14]A.Quarteroni C.Canuto, M.Y.Hussaini and T.A. Zang. *Spectral Methods in Fluid Dynamics; Springer Series in Computational Physics*. Springer Verlag, 1988.

A. APPENDIX

A. Matrix Operators for Numerical Differentiation

In this section we shall present a physical operator for numerical differentiation[13] of a periodic discrete function discussed over two parts. One for even number of discretization points and the other for odd. The results for even formulation can be found in[14] and is used extensively for computations using FFTs.

Let u be a function defined on the grid between $0 \leq x \leq 2\pi$,

$$x_j = \frac{2\pi j}{N} \qquad j = 0, 1, 2, ...N-1.$$

1. *Even Formulation*

Discrete Fourier transform of u is given by

$$\hat{u}_k = \frac{1}{N} \sum_{j=0}^{N-1} u(x_j) e^{-ikx_j}$$

and its inverse transform,

$$u(x_j) = \sum_{k=-\frac{N}{2}}^{\frac{N}{2}-1} \hat{u}_k e^{ikx_j}$$

The spectral derivative of u at the grid points is given by

$$(Du)_j = \sum_{k=-\frac{N}{2}+1}^{\frac{N}{2}-1} ik\hat{u}_k e^{ikx_j},$$

where we have set the Fourier coefficient corresponding to the oddball wave number equal to zero. Substituting for $\hat{u}_k$ from the Fourier transform, we obtain

$$(Du)_l = \frac{1}{N} \sum_{k=-\frac{N}{2}+1}^{\frac{N}{2}-1} \sum_{j=0}^{N-1} iku(x_j) e^{-ikx_j} e^{ikx_l}.$$

or

$$(Du)_l = \frac{1}{N} \sum_k \sum_j iku_j e^{\frac{2\pi ik}{N}(l-j)}.$$

Let

$$d_{lj} = \frac{1}{N} \sum_{k=-\frac{N}{2}+1}^{\frac{N}{2}-1} ike^{\frac{2\pi ik}{N}(l-j)} \tag{21}$$

Then

$$(Du)_l = \sum_{j=0}^{N-1} d_{lj} u_j$$

which expresses multiplication of a matrix with elements d_{lj} and the vector u. It turns out that d_{lj} can be computed analytically. To evaluate the sum in (21), recall that from geometric series, we have

$$S = \sum_{k=-\frac{N}{2}+1}^{\frac{N}{2}-1} e^{ikx} = e^{i(-\frac{N}{2}+1)x} + e^{i(-\frac{N}{2}+2)x} + ... + e^{i(\frac{N}{2}-1)x}$$

or

$$S = e^{i(-\frac{N}{2}+1)x}[1 + e^{ix} + e^{2ix} + ...e^{i(N-2)x}] = e^{i(-\frac{N}{2}+1)x}\frac{1 - e^{i(N-1)x}}{1 - e^{ix}}$$

or

$$S = \frac{e^{i(-\frac{N}{2}+1)x} - e^{i(\frac{N}{2})x}}{1 - e^{ix}} = \frac{e^{i(-\frac{N}{2}+\frac{1}{2})x} - e^{i(\frac{N}{2}-\frac{1}{2})x}}{e^{-i\frac{x}{2}} - e^{i\frac{x}{2}}} = \frac{\sin(\frac{N-1}{2}x)}{\sin\frac{x}{2}}$$

This expression can be differentiated to yield the desired sum

$$\frac{dS}{dx} = \sum_{k=-\frac{N}{2}+1}^{\frac{N}{2}-1} ike^{ikx} = \frac{(\frac{N-1}{2})\cos(\frac{N-1}{2}x)\sin\frac{x}{2} - \frac{1}{2}\cos\frac{x}{2}\sin(\frac{N-1}{2}x)}{(\sin\frac{x}{2})^2}$$

This expression can be simplified using trigonometric identities and noting that $x = \frac{2\pi}{N}(l-j)$,

$$\sin(\frac{Nx}{2} - \frac{x}{2}) = -(-1)^{l-j}\sin\frac{x}{2}$$

$$\cos(\frac{Nx}{2} - \frac{x}{2}) = (-1)^{l-j}\cos\frac{x}{2}$$

Therefore,

$$\frac{dS}{dx} = \frac{(\frac{N-1}{2})(-1)^{l-j}\cos\frac{x}{2}\sin\frac{x}{2} + \frac{1}{2}(-1)^{l-j}\cos\frac{x}{2}\sin\frac{x}{2}}{(\sin\frac{x}{2})^2}$$

or

$$\frac{dS}{dx} = \frac{\frac{N}{2}(-1)^{l-j}\cos\frac{x}{2}\sin\frac{x}{2}}{(\sin\frac{x}{2})^2} = \frac{N}{2}(-1)^{l-j}\cot\frac{x}{2}$$

Thus,

$$d_{lj} = \begin{cases} \frac{1}{2}(-1)^{l-j}\cot(\frac{\pi(l-j)}{N}) & : \quad l \neq j \\ 0 & : \quad l = j \end{cases}$$

With a change of variables, -m = (l-j), we have,

$$d_m = \begin{cases} \frac{1}{2}(-1)^{m+1}\cot(\frac{\pi m}{N}) & : \quad m \neq 0 \\ 0 & : \quad m = 0 \end{cases}$$

This change of variables shows that D is indeed a central difference operator since $d_{-m} = -d_m$

2. Odd Formulation

Discrete Fourier transform of u is given by

$$\hat{u}_k = \frac{1}{N}\sum_{j=0}^{N-1} u(x_j)e^{-ikx_j}$$

and its inverse transform,

$$u(x_j) = \sum_{k=-\frac{N-1}{2}}^{\frac{N-1}{2}} \hat{u}_k e^{ikx_j}$$

The spectral derivative of u at the grid points is given by

$$(Du)_j = \sum_{k=-\frac{N-1}{2}}^{\frac{N-1}{2}} ik\hat{u}_k e^{ikx_j}.$$

Note that for odd N there is no oddball element. Substituting for $\hat{u}_k$ from the Fourier transform, we obtain

$$(Du)_l = \frac{1}{N} \sum_{k=-\frac{N-1}{2}}^{\frac{N-1}{2}} \sum_{j=0}^{N-1} iku(x_j) e^{-ikx_j} e^{ikx_l}.$$

or

$$(Du)_l = \frac{1}{N} \sum_k \sum_j iku_j e^{\frac{2\pi ik}{N}(l-j)}.$$

Let

$$d_{lj} = \frac{1}{N} \sum_{k=-\frac{N-1}{2}}^{\frac{N-1}{2}} ike^{\frac{2\pi ik}{N}(l-j)} \tag{22}$$

Then

$$(Du)_l = \sum_{j=0}^{N-1} d_{lj} u_j.$$

To evaluate the sum in (22), we have

$$S = \sum_{k=-\frac{N-1}{2}}^{\frac{N-1}{2}} e^{ikx} = e^{i(-\frac{N-1}{2})x} + e^{i(-\frac{N-1}{2}+1)x} + ... + e^{i(\frac{N-1}{2})x}$$

or

$$S = e^{i(-\frac{N-1}{2})x}[1 + e^{ix} + e^{2ix} + ...e^{i(N-1)x}] = e^{i(-\frac{N-1}{2})x} \frac{1 - e^{iNx}}{1 - e^{ix}}$$

or

$$S = \frac{e^{i(-\frac{N-1}{2})x} - e^{i(\frac{N+1}{2})x}}{1 - e^{ix}} = \frac{e^{i(-\frac{N}{2})x} - e^{i(\frac{N}{2})x}}{e^{-i\frac{x}{2}} - e^{i\frac{x}{2}}} = \frac{\sin(\frac{N}{2}x)}{\sin\frac{x}{2}}$$

This expression will be differentiated to yield the desired sum

$$\frac{dS}{dx} = \sum_{k=-\frac{N-1}{2}}^{\frac{N-1}{2}} ike^{ikx} = \frac{(\frac{N}{2})\cos(\frac{N}{2}x)\sin\frac{x}{2} - \frac{1}{2}\cos\frac{x}{2}\sin(\frac{N}{2}x)}{(\sin\frac{x}{2})^2}$$

This expression can be simplified using trigonometric identities and noting that $x = \frac{2\pi}{N}(l-j)$,

$$\sin(\frac{Nx}{2}) = 0$$

$$\cos(\frac{Nx}{2}) = (-1)^{l-j}$$

Therefore,

$$\frac{dS}{dx} = \frac{(\frac{N}{2})(-1)^{l-j}\sin\frac{x}{2}}{(\sin\frac{x}{2})^2}$$

or

$$\frac{dS}{dx} = \frac{N}{2}(-1)^{l-j} cosec \frac{x}{2}$$

Thus,

$$d_{lj} = \begin{cases} \frac{1}{2}(-1)^{l-j} cosec(\frac{\pi(l-j)}{N}) & : \quad l \neq j \\ 0 & : \quad l = j \end{cases}$$

With a change of variables, -m = (l-j), we have,

$$d_m = \begin{cases} \frac{1}{2}(-1)^{m+1} cosec(\frac{\pi m}{N}) & : \quad m \neq 0 \\ 0 & : \quad m = 0 \end{cases}$$

The central difference operator form still holds for odd N.